Resistive and Conductive Tube Boundary Condition Models for Material Wire-Shaped Scatterers

Keith W. Whites, *Member, IEEE*

***Abstract*— An equivalent boundary condition model is introduced in this paper for computing the scattering by material wire-shaped scatterers which are either dielectric or magnetic, but not both simultaneously. While the methodology for numerically computing the scattering by perfectly conducting thin-wire scatterers has been developed for decades, no simple model for material scatterers with large length-to-radius ratios (wire shapes) has been available. This new model can be easily integrated into existing thin-wire computer codes while adding virtually no computational burden. Validating results are shown using comparisons of the full-wave scattering from a number of thin wire-shaped dielectric and magnetic structures with this new equivalent boundary condition model. It is demonstrated that this model is, in essence, an extension of the internal impedance expression for a conducting wire (developed over 50 years ago) to simple-material wire-shaped scatterers possessing a very wide range of material parameters.**

***Index Terms*—Electromagnetic scattering, wire scatterers.**

I. Introduction and Overview

A thin wire-scatterer, by definition, is a structure with a circular cross section and is very long with respect to the transverse dimension. The numerical computation of the scattering by such perfectly electrically conducting (PEC) structures was greatly aided by the introduction of the thin wire model (see, for example, [1]). Given that the aspect ratio is extremely large, a surface integral formulation of the scattering would be prohibitively expensive except for the most trivial of geometries.

The new model for material wire-shaped scatterers developed in this paper provides the same utility and computational savings as that achieved for PEC wires. Such a thin wire model for wire-shaped scatterers that are not PEC nor are highly lossy would be of value in such applications as scattering by vegetation, wave propagation along insulating wires, and in the modeling of complex composite materials [2]–[4]. At optical frequencies, the scattering by polymer strands would also be a practical use of this model. The first methodology for material wire scattering to appear in the literature (to our knowledge) was that developed by Newman [5]. As will be demonstrated later in this paper, the new model developed here gives the same level of accuracy as [5], but has the advantage of further simplicity and a satisfying relationship to existing models for conductive wires. However, a limitation of this new model that does not appear in [5] is that the material scatterer is either dielectric or magnetic, but not both simultaneously.

If the wire-shaped scatterer is very lossy, one may apply the impedance boundary condition (IBC) to formulate an accurate equivalent scattering problem [6]. Using this method, the scatterer is replaced by another of the same shape having null internal fields and a boundary condition on the surface

$$\hat{n} \times \overline{E} = Z_s \hat{n} \times \hat{n} \times \overline{H} \tag{1}$$

where $\hat{n}$ is the unit outward normal and Z_s is the surface impedance. As clearly dictated in [6], constraints need to be imposed on the scatterer for an accurate representation of the scattering using (1). These constraints are: 1) $|n_d| \gg 1$ where n_d is the index of refraction; 2) $|\mathrm{Im}(n_d)|k\rho \gg 1$ where ρ is the smallest radius of curvature or dimension; and 3) the penetration depth is sufficiently small such that no fields may pass through a given structure. From a study examining the scattering by two-dimensional (2-D) circular cylinders, it has been found that the loss criteria 2) and 3) are generally much more restrictive than the contrast criterion 1) [7].

Unfortunately, these restrictions may preclude the use of the IBC with thin material wire-shaped scatterers. In particular, considering a circular cross section, the restrictions 2) and 3) would place a larger lower bound on the loss for small diameter wires than for large ones.

In this paper, a new model for round material wire-shaped scatterers will be presented which is applicable regardless of the loss of the scatterer. In particular, accurate results are obtained for lossless bodies of virtually arbitrary constitutive parameters provided the typical thin-wire constraints are imposed. For lossless dielectric or magnetic scatterers, this new model is applicable provided $k_d a \lesssim 2.25$ where k_d is the wavenumber of the material wire and a is the wire radius. Since a is necessarily small, extremely large values of the constitutive parameters for the material cylinder are allowed.

The development of this new round material-wire scatterer model is given in the following section for dielectric-wire scatterers and in Section III for magnetic-wire scatterers. Results are shown in Section IV for a number of geometries that validate the accuracy of this model. Finally, in Section V, the behavior of this model is investigated in extreme values of the constitutive parameters and compared with known limiting cases. It will be shown that this new model is effectively an extension of the conductive wire boundary condition [8]–[13] to scatterers that may or may not be lossy.

Manuscript received January 4, 1996; revised June 17, 1996. This work was supported by the National Science Foundation under Grant ECS-9210551.

The author is with the Department of Electrical Engineering, University of Kentucky, Lexington, KY 40506 USA.

Publisher Item Identifier S 0018-926X(98)07504-8.

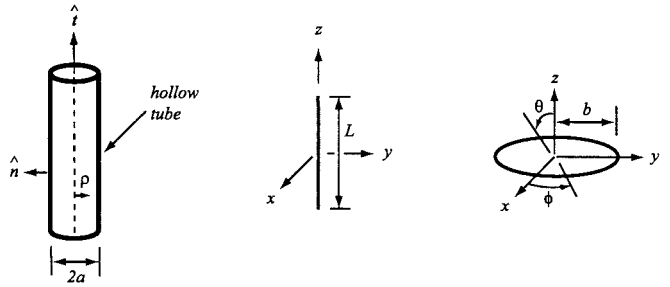

(a) (b) (c)

Fig. 1. Geometry of (a) the tube boundary condition model, (b) the material rod scatterer, and (c) the circular material loop scatterer.

II. Resistive Tube Boundary Condition Model

The structure chosen to equivalently model the scattering by dielectric wire-shaped objects is a "resistive tube." The development of this model will proceed from a 2-D analysis and will then be postulated to hold in three-dimensional (3-D) as well. Referring to Fig. 1(a), the resistive tube scatterer has the same circular cross section as the dielectric wire, is hollow inside, and has the boundary condition [14], [15]

$$\hat{n} \times [\overline{E}^+ - \overline{E}^-] = 0 \tag{2}$$

$$\hat{n} \times [\overline{E}^+ + \overline{E}^-] = 2R_s \hat{n} \times \hat{n} \times [\overline{H}^+ - \overline{H}^-] \tag{3}$$

imposed on the surface $\rho = a$. In (2) and (3), $\hat{n}$ is the unit normal in the "+" direction, and the "+" and "−" superscripts refer to surfaces at $\rho = a^+$ and a^-, respectively. While R_s (the complex surface resistivity) has a specific value for dielectric sheets [14], [15], it will be treated now as an unknown quantity.

Assume that a uniform plane wave is normally incident upon this scatterer polarized with the electric field parallel to the resistive tube cylinder (TM^z). The total fields internal and external to the resistive cylinder are, respectively, for $\rho \leq a$

$$E_z^T = E_0 \sum_{n=-\infty}^{\infty} j^{-n} q_n J_n(k\rho) e^{jn\phi} \tag{4}$$

$$H_\phi^T = -j \frac{E_o}{\eta} \sum_{n=-\infty}^{\infty} j^{-n} q_n J_n'(k\rho) e^{jn\phi} \tag{5}$$

where the prime indicates differentiation with respect to the argument, while for $\rho \geq a$

$$E_z^T = E_0 \sum_{n=-\infty}^{\infty} j^{-n} [J_n(k\rho) + p_n H_n^{(2)}(k\rho)] e^{jn\phi} \tag{6}$$

$$H_\phi^T = -j \frac{E_0}{\eta} \sum_{n=-\infty}^{\infty} j^{-n} [J_n'(k\rho) + p_n H_n^{(2)'}(k\rho)] e^{jn\phi} \tag{7}$$

assuming a suppressed time variation of $e^{j\omega t}$. The regions interior and exterior to the resistive tube have a wavenumber and characteristic impedance k and η, respectively. The coefficients p_n and q_n can be solved for by enforcing the boundary conditions that from (2) E_z is continuous giving

$$q_n J_n(ka) = J_n(ka) + p_n H_n^{(2)}(ka) \tag{8}$$

and that from (3) H_ϕ is discontinuous giving

$$q_n J_n(ka) = -R_s \frac{j}{\eta} \{J_n'(ka) + p_n H_n^{(2)'}(ka) - q_n J_n'(ka)\}. \tag{9}$$

The quantity of interest is p_n, which can be solved for using (8) and (9) such that

$$p_n = -\frac{J_n(ka) + j\theta_n \frac{R_s}{\eta} J_n'(ka)}{H_n^{(2)}(ka) + j\theta_n \frac{R_s}{\eta} H_n^{(2)'}(ka)} \tag{10}$$

where

$$\theta_n = \frac{J_n(ka)}{J_n(ka) - j \frac{R_s}{\eta} J_n'(ka)}. \tag{11}$$

The utility of the resistive tube model is the ability to accurately represent the scattered fields external to a dielectric cylinder. This can be accomplished exactly for the circular 2-D cylinder by equating the scattered fields given in (6) and (7) with those of a dielectric cylinder and solving for the *equivalent* surface resistivity.

For the same plane wave illumination as above, the total fields external to the material cylinder can easily be found following a procedure similar to that in [16, ch. 5]

$$E_z^T = E_0 \sum_{n=-\infty}^{\infty} j^{-n} [J_n(k\rho) + a_n H_n^{(2)}(k\rho)] e^{jn\phi} \tag{12}$$

where

$$a_n = -\frac{J_n(ka) - \eta_r \frac{J_n(k_d a)}{J_n'(k_d a)} J_n'(ka)}{H_n^{(2)}(ka) - \eta_r \frac{J_n(k_d a)}{J_n'(k_d a)} H_n^{(2)'}(ka)}. \tag{13}$$

Here

$$k_d = \omega\sqrt{\mu\varepsilon_d} = k\sqrt{\varepsilon_r} \quad \text{and} \quad \eta_r = \frac{\eta_d}{\eta} = \sqrt{\frac{1}{\varepsilon_r}} \tag{14}$$

with μ and ε_d the constitutive parameters of the cylinder. Equating (6) and (12) term-by-term leads to the requirement that

$$-\eta_r \frac{J_n(k_d a)}{J_n'(k_d a)} = j\theta_n \frac{R_{sn}}{\eta} \tag{15}$$

or

$$R_{sn} \equiv R_s(n) = \frac{j\eta_d}{\frac{J_n'(k_d a)}{J_n(k_d a)} - \eta_r \frac{J_n'(ka)}{J_n(ka)}}. \tag{16}$$

From this last equation, it can be seen that in order for the resistive tube cylinder to exactly model the scattering by a dielectric cylinder, the equivalent surface resistivity must be a function of n. However, for certain small diameter material cylinders (in terms of wavelength in the surrounding material) the scattering will be dominated by the $n = 0$ term leading

to the approximate equivalent surface resistivity for dielectric wires

$$R_s \approx \frac{j\eta_d}{\eta_r \dfrac{J_1(ka)}{J_0(ka)} - \dfrac{J_1(k_d a)}{J_0(k_d a)}}. \tag{17}$$

This azimuthally symmetric scattering assumption will prescribe limits (given in Section IV) on the dielectric wire material parameters for a valid application of this model. Strictly speaking, the equivalent surface resistivity in (17) is only valid for infinite 2-D cylinders. However, it will be hypothesized that this model and the resistivity expression (17) remain approximately valid for a certain class of finite, 3-D shaped dielectric structures. In particular, evidence for the validity of this hypothesis for thin wire-shaped scatterers is presented in the next section.

Implementation of this resistive tube boundary condition (RTBC) model for wire-shaped dielectric scatterers into a frequency-domain integral equation solution for the scattering is very similar to PEC scatterers [1]. Provided the length of the scatterer is much greater than the radius and that the radius is much smaller than a wavelength in the surrounding material, the equivalent current is assumed to be only axially varying and possesses no azimuthal variation. Additionally, the equivalent currents on the endcaps are ignored. Construction of the electric field integral equation (EFIE) proceeds by enforcing the relation

$$\hat{n} \times \overline{E}^I(\overline{r}) = \hat{n} \times \overline{E}^T(\overline{r}) - \hat{n} \times \overline{E}^S(\overline{r}) \tag{18}$$

for $\overline{r} \in \{\text{points on tube}\}$ where the superscripts I and S refer to the incident and scattered fields, respectively. Employing the RBC (2) and (3) on the surface of the tube, using R_s from (17), gives the EFIE for the axial component t of the field

$$E_t^I(t) = R_s J_t(t) - \hat{t} \cdot \overline{E}^S(t) \tag{19}$$

or for the equivalent electric current along the surface of the wire $I(t)$ using a mixed potential source/field relationship

$$E_t^I(t) = \frac{R_s}{2\pi a} I(t) + jk\eta A_t(t) + \hat{t} \cdot \nabla \Phi_e(t). \tag{20}$$

The unit vector $\hat{t}(t)$ points along the axis of the wire structure and varies with parameter t along the wire. Assuming that $\hat{n} \times \overline{E}$ is approximately constant within the tube, this current can be assumed to exist, in the usual fashion, as a filament along the axis of the scatterer. Again, this approximation would be reasonable for long, thin, wire-shaped scatterers. Equation (20) is very similar to the standard EFIE for PEC wire scatterers other than the additional term containing R_s.

Two of the most appealing attributes of this RTBC model are the negligible computational cost and the ease at which it can be integrated into existing PEC wire scattering codes. Both of these attributes can be established by considering the formation of the system of equations used in a moment method (MM) solution. Expanding the current in a set of basis functions B_n and forming the inner product of (20) with a testing function T_m along the contour C of the wires where $m, n = 1, \cdots, N$, gives

$$\langle T_m, E_t^I(t) \rangle_C = \frac{1}{2\pi} \left\langle T_m, \frac{R_s}{a} I(t) \right\rangle_C + jk\eta \langle T_m, A_t(t) \rangle_C + \langle T_m, \hat{t} \cdot \nabla \Phi_e(t) \rangle_C. \tag{21}$$

It is apparent that the first term in the right-hand side of (21) is nonzero only when the basis and testing functions overlap. For example, using a pulse-expansion/point-match solution, only terms on the main diagonal of the impedance matrix would be modified beyond that for PEC wires, while a triangle expansion/pulse test would modify the main diagonal plus the two adjacent off-diagonal terms in each row.

III. Conductive Tube Boundary Condition Model

The development of the equivalent model for the scattering by magnetic wires ($\varepsilon_r = 1$, $\mu_r \neq 1$) proceeds in a like manner as that discussed in the previous section for dielectric wires. However, duality can be invoked to expedite this development since both Maxwell's equations and the boundary conditions for the two types of material scatterers are dual.

Applying duality ($\overline{E} \to \overline{H}$, $\overline{H} \to -\overline{E}$, $\eta \to 1/\eta$) to (2) and (3) yields what has been labeled the (magnetically) conductive sheet boundary condition [15], [17]

$$\hat{n} \times [\overline{H}^+ - \overline{H}^-] = 0 \tag{22}$$

$$\hat{n} \times [\overline{H}^+ + \overline{H}^-] = -2R_s^* \hat{n} \times \hat{n} \times [\overline{E}^+ - \overline{E}^-] \tag{23}$$

where R_s^* is the complex surface conductivity. The scattered fields external to a conductive tube having these boundary conditions under TE^z illumination can be equated with those of a round magnetic material cylinder, similar to the last section, to yield the equivalent conductive tube boundary condition (CTBC) for magnetic wire-shaped scatterers. Alternatively, applying duality to (17) yields

$$R_s^* \approx \frac{j/\eta}{\dfrac{J_1(ka)}{J_0(ka)} - \eta_r \dfrac{J_1(k_d a)}{J_0(k_d a)}}. \tag{24}$$

Implementation of this CTBC for magnetic wire-shaped scatterers into an integral equation solution proceeds in a dual fashion to the development presented in the last section. Applying duality to (18) gives

$$\hat{n} \times \overline{H}^I(\overline{r}) = \hat{n} \times \overline{H}^T(\overline{r}) - \hat{n} \times \overline{H}^S(\overline{r}) \tag{25}$$

while applying duality to (20) or, alternatively, applying the boundary conditions (22) and (23), yields the magnetic field integral equation

$$H_t^I(t) = \frac{R_s^*}{2\pi a} I^*(t) + j \frac{k}{\eta} F_t(t) + \hat{t} \cdot \nabla \Phi_m(t) \tag{26}$$

where I^* is the equivalent magnetic current along the wire, F_t is the tangential electric vector potential, and Φ_m is the scalar magnetic potential. This integral equation can be numerically solved by expanding I^* in a basis set and testing as in (21). Comparing (20) with (26), however, it is noted that the same computer code can be used to solve the magnetic material wire-shaped scattering problem (CTBC) as that used for dielectric wire-shaped geometries (RTBC) provided $\eta \to 1/\eta$

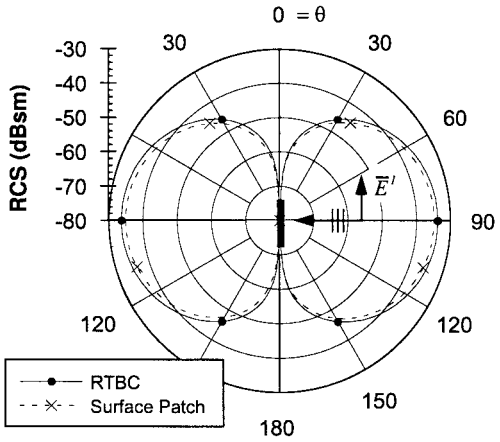

Fig. 2. Bistatic RCS comparison in the $y = 0$ plane of Fig. 1(b) for a rod material wire scatterer of wire radius $= a = 0.0075$ m and length $= L = 0.75$ m with $\varepsilon_r = 15$ and $\mu_r = 1$ at $f = 300$ MHz. The TM^z polarized plane wave is normally incident to the rod at $\theta^{\text{inc}} = 90°$, $\phi^{\text{inc}} = 0°$.

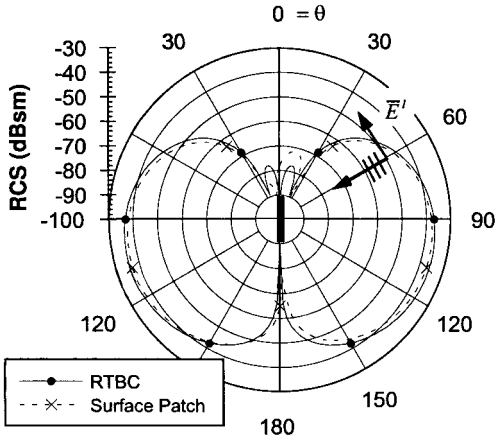

Fig. 3. Bistatic RCS comparison in the $y = 0$ plane of Fig. 1(b) for the rod material wire scatterer of Fig. 2. The TM^z polarized plane wave is obliquely incident to the rod at $\theta^{\text{inc}} = 60°$, $\phi^{\text{inc}} = 0°$.

in the latter code. A mixture of dielectric and magnetic wire-shaped scatterers would require additional code modifications.

IV. Validating Results and Limits of Applicability

Two types of validating comparisons will be given. The first type is a far-field comparison between the RTBC and CTBC models and the scattering by 3-D volumetric shapes as computed using a surface integral equation approach. The material-wire scattering was computed using the integral equations (20) and (26) with a triangle basis function expansion and pulse testing as developed in [18]. The natural boundary condition of zero current at the ends of the material wires was enforced, contrary to the development in [5]. The scattering by the 3-D volumetric shapes was computed using the Poggio *et al.*(PMCHW) integral equation formulation with flat triangular vector basis functions [19], [20].

For these comparisons, two material wire-shaped bodies were considered. Shown in Figs. 2 and 3 is the bistatic RCS for a straight dielectric rod of $a =$ radius $= 0.0075$ m and L $=$ length $= 0.75$ m, orientated as in Fig. 1(b), with $\varepsilon_r = 15$ and $\mu_r = 1$ at $f = 300$ MHz. In Fig. 2 the TM^z polarized plane wave is "normally" incident at $\theta^{\text{inc}} = 90°$, $\phi^{\text{inc}} = 0°$ and the scattered field is observed at θ in the $y = 0$ plane. In Fig. 3, the TM^z polarized plane wave is "obliquely" incident at $\theta^{\text{inc}} = 60°$, $\phi^{\text{inc}} = 0°$. The scattered fields in the $x = 0$ plane (not shown) were observed to have nearly the same agreement for both of these examples.

Shown in Figs. 4 and 5 are the comparisons of the bistatic RCS for a circular dielectric-wire loop of radius 0.12 m and $a = 0.0075$ m, orientated as in Fig. 1(c), with $\varepsilon_r = 15$ and $\mu_r = 1$ at $f = 300$ MHz. In Fig. 4, the TE^z plane wave is incident at $\theta^{\text{inc}} = \phi^{inc} = 0°$, while in Fig. 5, the plane wave is incident at $\theta^{\text{inc}} = 30°$, $\phi^{inc} = 0°$. Shown in Fig. 6 is the monostatic scattering by a TE^z plane wave in the plane $y = 0$ incident on the same loop.

Because of duality, the results from the comparison of the CTBC model for magnetic material wire-shaped scatterers and the surface patch results can be ascertained from Figs. 2–6. In

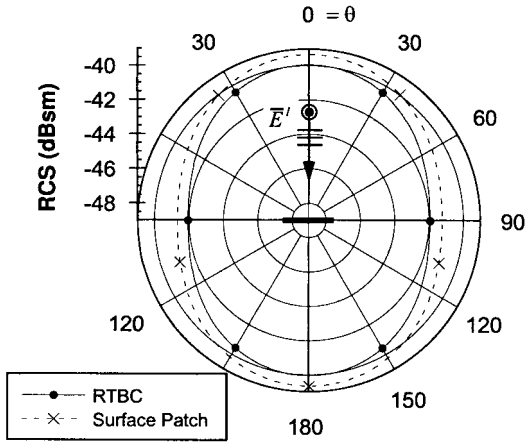

(a)

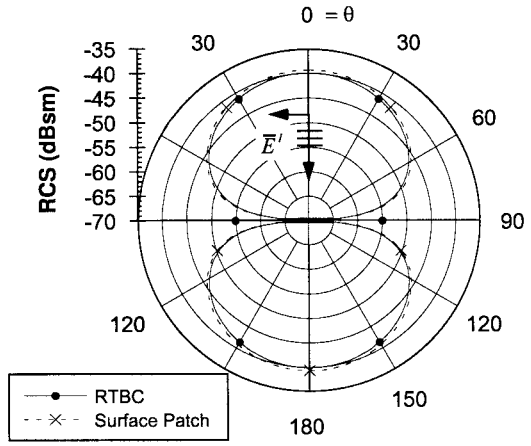

(b)

Fig. 4. Bistatic RCS comparison in the (a) $y = 0$ and (b) $x = 0$ planes of Fig. 1(c) for a circular thin-wire material loop scatterer of radius $= b = 0.12$ m and $a = 0.0075$ m with $\varepsilon_r = 15$ and $\mu_r = 1$ at $f = 300$ MHz. The TE^z polarized plane wave is normally incident to the loop at $\theta^{\text{inc}} = \phi^{\text{inc}} = 0°$.

particular, Figs. 2 and 3 pertain to TE^z plane-wave scattering by a material rod with constitutive parameters $\varepsilon_r = 1$ and $\mu_r = 15$ while Figs. 4–6 pertain to TE^z plane-wave scattering by a magnetic material loop also with constitutive parameters

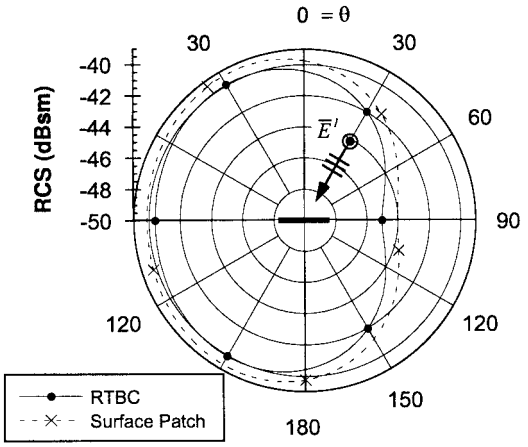

(a)

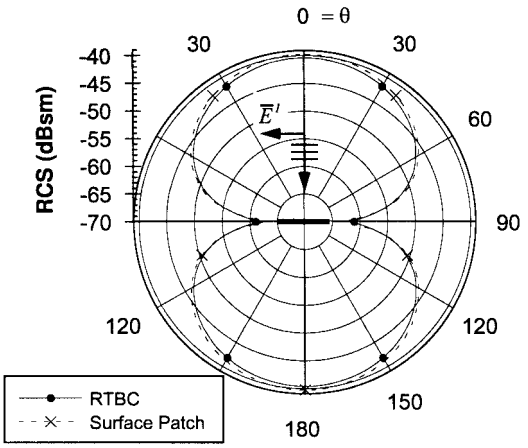

(b)

Fig. 5. Bistatic RCS comparison in the (a) $y = 0$ and (b) $x = 0$ planes of Fig. 1(c) for the circular thin-wire material loop scatterer of Fig. 4. The TE^z polarized plane wave is obliquely incident to the loop at $\theta^{\text{inc}} = 30°$ and $\phi^{\text{inc}} = 0°$.

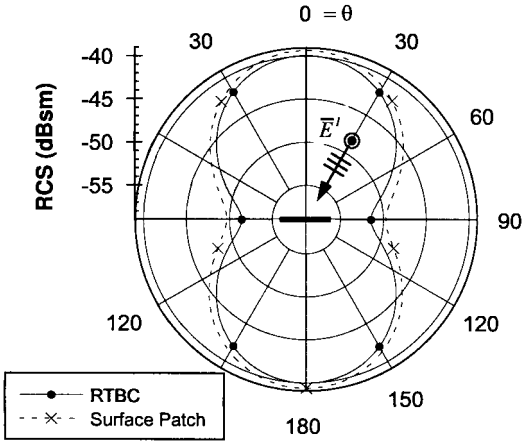

Fig. 6. Monostatic RCS comparison for the circular, thin-wire material loop of Fig. 4. The TE^z polarized plane wave is incident in the $y = 0$ plane of Fig. 1(c).

$\varepsilon_r = 1$ and $\mu_r = 15$. These results were confirmed using the RTBC computer code (with $\eta \to 1/\eta$ as mentioned in the previous section) and the surface patch code with TE^z illumination and the magnetic material parameters.

Because of the high-aspect ratio, the number of unknowns in the PMCHW MM surface-patch solution was quite large. To keep the problem within a manageable size, the surface patch model had a pentagon cross section with a total of 2256 unknowns (nonboundary edges with 378 nodes and 752 triangular elements) for the rod and 3180 unknowns (530 nodes and 1060 triangular elements) for the loop. Some error is expected in this surface-patch solution due to the faceting approximation and the fact that the radar cross section (RCS) is approaching the "noise floor" of this PMCHW model using the same vector basis function expansions for the equivalent surface electric and magnetic currents. Nevertheless, the agreement in the far-scattered fields of Figs. 2–6 is close—within approximately 1 dB or less. This agreement in the far-scattered fields is achieved at an enormous reduction in the computational expense since only 49 triangular basis functions were used in the RTBC rod solution in Figs. 2 and 3 while 100 triangular basis functions were used in the RTBC loop solution in Figs. 4–6.

The second type of comparison is between the RTBC and CTBC models and an infinite 2-D circular cylinder. Shown in Fig. 7(a) is the backscattered RCS for TM^z plane-wave illumination at "normal" incidence ($\theta^{\text{inc}} = 90°$, $\phi^{inc} = 0°$) for a dielectric cylinder with $a = 0.01$ m and $L = 2$ m at $f = 300$ MHz using 99 triangular basis functions. The 2-D circular cylinder results were obtained using (12) and (13) with the appropriate far-field simplifications. The resulting echo width was scaled by the factor [5]

$$\text{RCS} = \frac{2L^2}{\lambda} \cdot (\text{echo width}). \tag{27}$$

This comparison illustrates the wide range of material parameters for which this RTBC model applies. The data shown in Fig. 7(a) agrees nearly identically with that given in Fig. 5 of [5]. Similar agreement was found when varying the conduction loss of the cylinder as given in Fig. 4 of [5].

However, extending the range of the cylinder permittivity yields the results shown in Fig. 7(b). While the relative permittivity range in this figure is quite large, it is not physically unrealistic. Barium strontium titanate helices in [21], manufactured for chiral materials research, had a reported dielectric constant of 1000–1500 at microwave frequencies. From Fig. 7(b) it is quite obvious that the RTBC model fails to accurately predict the scattering of the scaled eigenfunction solution near a certain "resonance" occurring at $\log_{10}(\varepsilon_r) = 3.1658$. It can be analytically shown from (12) using (13) that near this permittivity value, the harmonic terms $n = 0, 1$, and -1 all contribute the same order of magnitude to the scattered fields external to the cylinder. In fact, at the center resonance value of $\varepsilon_r = 1464.9$ where

$$J_0(k_d a) = 0 \tag{28}$$

then $a_0 = a_1 = a_{-1}$. Therefore, it is no surprise that the RTBC model fails to predict the scattering near the resonance since this thin-wire modeling assumes that the longitudinally induced current is axially symmetric and that only the $n = 0$ harmonic contributes significantly to the scattering. Since both the $n = \pm 1$ harmonics contribute

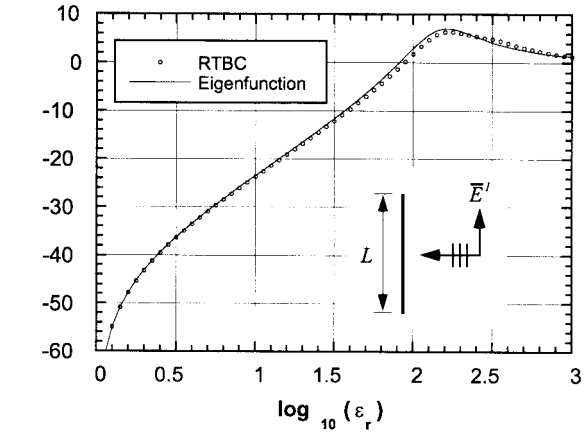

(a)

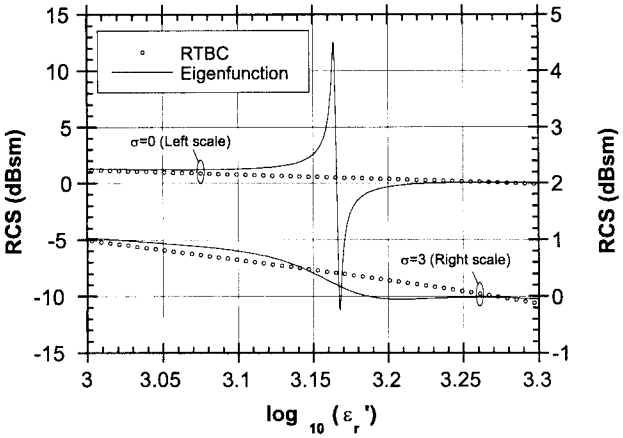

(b)

Fig. 7. Backscattered RCS comparison for a dielectric rod wire scatterer with $a = 0.01$ m and $L = 2$ m for $\mu_r = 1$ at $f = 300$ MHz (a) $\sigma = 0$ and (b) $\sigma = 0$, 3 S/m. The TM^z polarized plane wave is normally incident to the rod at $\theta^{\rm inc} = 90°$, $\phi^{\rm inc} = 0°$.

significantly to the scattering, no thin-wire model based on azimuthally symmetric current assumptions will yield correct scattering predictions near this resonance. As the loss, σ, of the cylinder is increased following $\varepsilon_r = \varepsilon_r' - j\sigma/\omega\varepsilon_0$, this resonance is greatly dampened as attested by the results in Fig. 7(b) with $\sigma = 3$ S/m.

Based on these findings, and other numerical experimentation, the RTBC model has been determined to accurately predict the scattering by wire-shaped dielectric objects provided

$$|a_0| \gg |a_1|. \tag{29}$$

With $\sigma = 3$ and $\varepsilon_r' = 1465$ in Fig. 7(b), $|a_0|/|a_1| \approx 27.5$. In the case of lossless material wires, further simplification of (29) can be obtained using (28) and Fig. 7 to give the region of validity of the RTBC model as

$$k_d a \lesssim 2.25. \tag{30}$$

Since these wire-shaped scatterers will necessarily have small radii, a, the allowed values of the constitutive parameters can be quite large as seen in the results of Fig. 7.

By duality, the data in Fig. 7 also pertain to a magnetic material rod scatterer with TE^z plane-wave illumination and $\varepsilon_r \leftrightarrow \mu_r$. Hence, the limitations of the CTBC model for magnetic wire-shaped scatterers are identical to those for the RTBC model and dielectric wire-shaped scatterers given in (29) and (30). This finding and the resonance behavior have both been verified using the eigenfunction solution for TE^z scattering by a round magnetic material cylinder and the CTBC material wire scattering code.

V. Discussion and R_s Behavior

The comparisons displayed in the last section present compelling evidence for the accuracy of the RTBC and CTBC models for material wire-shaped scatterers. In this section, attention will be focused on the expression for R_s in (17). In particular, a few physically meaningful properties will be examined and, where appropriate, compared to results obtained by others.

The first property to be examined from (17) is when the material is lossless. In such cases, R_s is purely imaginary. Applying Poynting's theorem to a resistive sheet with surface current density $\overline{J}_s$ it can be easily shown that the time-averaged power absorbed by the sheet is given by

$$\langle P_{abs} \rangle = \tfrac{1}{2} \int_S \mathrm{Re}(R_s) |\overline{J}_s|^2 \, ds. \tag{31}$$

Hence, if R_s is purely imaginary, there will be no time-averaged power absorbed in the RTBC model as required. Conversely, from (31) time-averaged power absorption would be expected when R_s is complex which is precisely the outcome when the scatterer becomes lossy as seen in (17).

The second property of the RTBC model to be examined is the limit when the scatterer is a "good" conductor. One of the earliest works pertaining to the numerical computation of scattering by finite wires of finite conductivity was Cassedy and Fainberg [10]. They employed a boundary condition for the ratio of the total longitudinal electric field and current

$$Z_i \equiv \frac{E_t(a)}{I(a)} = \frac{1}{a}\sqrt{\frac{f\mu}{j2\pi\sigma}} \frac{J_0\left(a\sqrt{\frac{\omega\mu\sigma}{j}}\right)}{J_1\left(a\sqrt{\frac{\omega\mu\sigma}{j}}\right)} \tag{32}$$

derived from a two-dimensional round lossy cylinder provided $\sigma \gg \omega\varepsilon$. While Cassedy and Fainberg reference this equation from [9], King presented this same result four years earlier [8].

Sometime later, improvements to the computation of the scattering by lossy wire structures was developed in [11]–[13]. However, these improvements involved only the numerical solution methodology while the internal surface impedance expression used remained the same as (32). Under the condition that

$$\frac{J_1(k_d a)}{J_0(k_d a)} \gg \eta_r \frac{J_1(ka)}{J_0(ka)} \tag{33}$$

which is wholly satisfied if the scatterer is a good conductor, then the internal impedance defined as

$$Z^i \equiv \frac{R_S}{2\pi a} \tag{34}$$

using (17) becomes

$$Z^i \approx -j\,\frac{\eta_d}{2\pi a}\,\frac{J_0(k_d a)}{J_1(k_d a)} \tag{35}$$

which is identical to (32). Hence, the RTBC model reduces to the accepted model for lossy wires provided the scatterer is a "good" conductor. In the small argument limit ($k_d a \to 0$) when the frequency or wire radius become very small, then from (35) $Z^i \approx 1/\pi a^2 \sigma$, which is the typical expression for the per unit length dc resistance of a wire, as expected. Furthermore, from (17) in the limit as σ becomes very large (regardless of frequency), Z^i approaches zero as would be expected for PEC scatterers.

VI. Summary and Conclusions

New boundary condition models have been developed in this paper for wire-shaped scatterers that are composed of a material which may or may not be lossy. These new models provide the same level of accuracy and computational savings as the widely used formulation for PEC thin-wire scatterers. Furthermore, these RTBC and CTBC models can be added to an existing PEC thin-wire code (within the moment method matrix fill) with little effort while adding only a negligible computational burden to the code.

These new models were subjected to a number of validating tests. In Section IV, the scattering by straight rods and circular loops were favorably compared to the full-wave surface-patch moment-method solutions. Also, the scaled scattering by a round 2-D cylinder was compared to the RTBC (CTBC) results of a long straight rod as the relative permittivity (permeability) of the lossless cylinder varied from nearly one to over 1000. The results of this comparison demonstrate the extremely wide range of material constants for which the scattering may be accurately predicted using the two models. In particular, it was shown in Section IV that the RTBC and CTBC models are applicable to lossless material wire-shaped bodies satisfying the constraint $k_d a \lesssim 2.25$ where k_d is the wavenumber of the material composing the wire and a is the wire radius. Since a is necessarily small, then the material-wire constitutive parameters can be very large. For lossy material wires, the requirement (29) must be satisfied.

Finally, it was shown in Section V that in the limit as the scatterer becomes a good conductor, the RTBC model reduces to that used for more than five decades for lossy conductors. However, this RTBC model also pertains to dielectric scatterers which are not conductors at all (that is, lossless) as demonstrated in Section IV. Therefore, this RTBC model (17), (19) can be viewed as essentially an extension of the internal impedance expression (32)—given by King some 50 years ago—to wire-shaped dielectric scatterers composed of simple media and possessing a very wide range of material parameters.

References

[1] R. F. Harrington, *Field Computation by Moment Methods.* Malabar, FL: Krieger, 1968.

[2] K. W. Whites, "Host effects on the constitutive parameters for synthetic chiral media," in *Proc. Chiral'94*, Perigueux, France, May 1994, pp. 77–82.

[3] ——, "Computation and physical behavior of bi-isotropic material parameters for a class of lossy inclusions," in *Dig. URSI Radio Sci. Int. Symp.*, Seattle, WA, June 1994, p. 428.

[4] ——, "Full-wave computation of constitutive parameters for lossless composite chiral materials," *IEEE Trans. Antennas Propagat.*, vol. 43, pp. 376–384, Apr. 1995.

[5] E. H. Newman, "A unified theory of thin material wires," *IEEE Trans. Antennas Propagat.*, vol. 39, pp. 1488–1496, Oct. 1991.

[6] T. B. A. Senior, "Impedance boundary conditions for imperfectly conducting surfaces," *Appl. Sci. Res.*, vol. 8, Sec. B, pp. 418–436, 1960.

[7] K. W. Whites, "Electromagnetic scattering simulations using equivalent boundary condition models," Ph.D. dissertation, Univ. Illinois, Urbana/Champaign, 1991.

[8] R. W. P. King, *Electromagnetic Engineering.* New York: McGraw-Hill, 1945.

[9] S. Ramo and J. R. Whinnery, *Fields and Waves in Modern Radio.* New York: Wiley, 1949.

[10] E. S. Cassedy and J. Fainberg, "Back scattering cross sections of cylindrical wire of finite conductivity," *IRE Trans. Antennas Propagat.*, vol. AP-8, no. 1, pp. 1–7, Jan. 1960.

[11] C. D. Taylor, C. W. Harrison Jr., and E. A. Aronson, "Resistive receiving and scattering antenna," *IEEE Trans. Antennas Propagat.*, vol. AP-15, no. 3, pp. 371–376, May 1967.

[12] J. H. Richmond, "Scattering by imperfectly conducting wires," *IEEE Trans. Antennas Propagat.*, vol. AP-15, no. 6, pp. 802–806, Nov. 1967.

[13] E. S. Cassedy and J. Fainberg, "Comments, with reply, on 'Resistive receiving and scattering antenna,'" *IEEE Trans. Antennas Propagat.*, vol. AP-16, no. 1, pp. 128–129, Jan. 1968.

[14] R. F. Harrington and J. R. Mautz, "An impedance sheet approximation for thin dielectric shells," *IEEE Trans. Antennas Propagat.*, vol. AP-23, no. 4, pp. 531–534, July 1975.

[15] T. B. A. Senior, "Combined resistive and conductive sheets," *IEEE Trans. Antennas Propagat.*, vol. AP-33, pp. 577–579, May 1985.

[16] R. F. Harrington, *Time-Harmonic Electromagnetic Fields.* New York: McGraw-Hill, 1961.

[17] T. B. A. Senior, "Approximate boundary conditions," *IEEE Trans. Antennas Propagat.*, vol. AP-29, pp. 826–829, May 1981.

[18] A. W. Glisson and D. R. Wilton, "Simple and efficient numerical methods for problems of electromagnetic radiation and scattering from surfaces," *IEEE Trans. Antennas Propagat.*, vol. AP-28, pp. 593–603, May 1980.

[19] K. Umashankar, A. Taflove, and S. M. Rao, "Electromagnetic scattering by arbitrary shaped three-dimensional homogeneous lossy dielectric objects," *IEEE Trans. Antennas Propagat.*, vol. AP-34, pp. 758–766, June 1986.

[20] S. M. Rao, D. R. Wilton, and A. W. Glisson, "Electromagnetic scattering by surfaces of arbitrary shape," *IEEE Trans. Antennas Propagat.*, vol. AP-30, pp. 409–418, Mar. 1982.

[21] F. Guérin, V. K. Varadan, V. V. Varadan, M. Labeyrie, and P. Y. Guillon, "Some experimental results on the dispersive behavior of chiral composites," *J. Phys. D: Appl. Phys.*, vol. 28, no. 1, pp. 194–201, 1995.

Keith W. Whites (S'84–M'91) was born in Huron, SD. He received the B.S.E.E. degree from the South Dakota School of Mines and Technology, Rapid City, in 1986, and the M.S. and Ph.D. degrees from the University of Illinois, Urbana/Champaign, in 1988 and 1991, respectively.

In 1986, he was a Graduate Summer Assistant at Sandia National Laboratories, Livermore, CA. From 1987 to 1988 he was a Research Assistant with the United States Army CERL, Champaign, IL, where he conducted research in electromagnetic compatibility issues related to shielding. From 1988 to 1991 he held various fellowships and assistantships within the Department of Electrical and Computer Engineering at the University of Illinois, including Lecturer for the academic year 1990–1991. Since 1991 he has been at the University of Kentucky where he is currently an Associate Professor of Electrical Engineering teaching courses in theoretical and numerical electromagnetics, among other topics. His research interests include the theoretical and numerical modeling of electromagnetics problems, effective media descriptions for complex composite materials, numerical simulation of the electrophotography process, electromagnetic shielding, and radar cross-section reduction.

Dr. Whites is a 1996 recipient of the National Science Foundation Faculty Early Career Development (CAREER) Award and is a member of Tau Beta Pi and Eta Kappa Nu.